ACS APPLIED MATERIALS & INTERFACES

Research Article

www.acsami.org

Micrometer-Sized Fluorine Doped Tin Oxide As Fast Electron Collector for Enhanced Dye-Sensitized Solar Cells

Xiao Rui Cui,[†] Ye Feng Wang,[‡] Zhao Li,[†] Lu Zhou,[†] Fei Gao,[†] and Jing Hui Zeng*[,†]

[†]School of Materials Science and Engineering, [‡]School of Chemistry and Chemical Engineering & Key Laboratory of Macromolecular Science of Shaanxi Province, Shaanxi Normal University, Xi'an, China, 710119

Supporting Information

ABSTRACT: Titanium dioxide (TiO_2)-layered fluorine doped tin oxide (FTO) powder was synthesized and applied as the photoanode in dye-sensitized solar cells (DSSCs). FTO powders are connected to form a direct electron pathway for the efficient extract of injected electrons, while the TiO_2 layer serves as an energy barrier prohibiting the charge combination with oxidized dye or I_3^-. The electrochemical impedance spectroscopy (EIS) analyses suggest that electrons have a longer combination lifetime (τ_e = 233 ms) than that of the electron in the DSSCs using traditional P25 photoanodes (τ_e = 28 ms). The DSSCs using 5 μm thick TiO_2@FTO as photoanodes eventually give a respectable and long-term stable photovoltaic performance with a current density of 23.8 mA/cm^2, an open circuit voltage of 0.69 V, and power conversion efficiency of 7.4%. The results are received on a low dye loading level (0.25×10^{-7} mol/cm^2), which is $^1/_{10}$ of that for traditional photoanode (2.79×10^{-7} mol/cm^2).

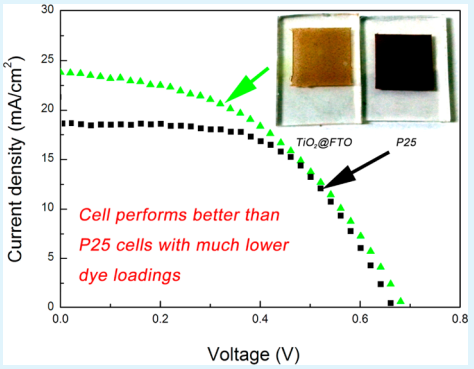

KEYWORDS: *FTO powder, dye-sensitized solar cell, electron lifetime, collection, efficiency*

INTRODUCTION

One important issue for dye-sensitized solar cells (DSSCs) is the enhancement of the charge transport and collection efficiency.[1−3] Although long lifetimes for photogenerated charges are due to electrons and holes residing in different phases,[4] the electrons injected into metal oxide photoanodes are prone to recombine with oxidized species, typically I_3^-, in electrolytes if they are not transported and collected in an efficient way. Unfortunately, electrons in photoanodes made from metal oxide semiconductor nanoparticles do not travel in the drift mode. Instead, they are transported in the much slower paces of "random walking"[5] or ambipolar diffusion[6] mode, owing to the neutralization of electrons with the ions in the electrolyte,[7,8] or by surface traps in the nanoparticles.[9] Many research works have reported an increasing charge transport and collection efficiency.[10−12]

The methods for a higher charge transportation rate and better collection efficiency can be classified into three major strategies: The first one is to provide a direct electron transport channel using one-dimensional (1D) nanowires/nanotubes to avoid the electron random walking in the nanoparticle layers.[6,13] Although the 1D structure favors the electron migration, the apparent lesser surface area of these 1D structures results in less dye loading, which balances the efficiency.[14] Better efficiencies are reported for cells with alternate techniques such as ultralong nanowires[15] or nanowire/nanoparticle composites,[16] but the efficiencies are still not competitive with those from nanoparticle photoanodes.

The second tactic is to increase the intrinsic electron mobilities either by doping the TiO_2 nanoparticles[17] or by applying semiconductor with higher electron mobility, such as ZnO[15] or SnO_2[18] for the photoanodes. Although doping results in the higher charge mobility than undoped TiO_2,[19] it also affects the visible-infrared transparency to reduce the dye absorbance as a consequence.[20] Increased short-circuit current density is received by the higher electron mobility with doped photoanodes; however, the advantage is also withdrawn by the reduced open-circuit voltage.[21,22] The alternates of TiO_2 in photoanodes face other problems. ZnO is not stable in an acid environment, and the SnO_2 surface (the isolectric point pH 4−5) is difficult to absorb the Ru dye carrying carboxyl attachment groups.[23] An extra metal oxide layer is provided on the ZnO or SnO_2 surfaces to avoid these problems.

The third tactic is to shrink electron transport distance in photoanodes, which apparently shorten electron collection distance. As a result, electrons migrate to the outer circuit efficiently to provide enhanced power output. Nickel pillars and carbon coatings are applied for this target. Due to the lesser surface area for dye loading after carbon coating, cell efficiencies of less than 6% are reported.[3,24] Along with a high conductivity, Ag nanoscale structures are applied for photoanode.[25,26] We demonstrated a cell efficiency enhancement of over 37% with Ag/TiO_2 nanowire loading compared to mere P25 photoanode cells.[27] Carbon coated silver nanowires are reported to protect silver from corrosion by iodine electrolyte while maintain high conductivity.[28] Furthermore, indium tin oxide (ITO)[29] and

Received: May 19, 2014
Accepted: September 16, 2014
Published: September 16, 2014

fluorine doped tin oxide (FTO)[30] thin film as conducting oxides coated on the surface TiO_2 or ZnO nanowries photoanode films for DSSCs exhibited better performance than pure TiO_2 photoanode films. Recently, some researchers reported DSSC devices based on titania-coated FTO nanoparticles replacing TiO_2 nanoparticles as photoanodes with conversion efficiencies ranging from 3.8 to 4.8%.[31,32] Despite their specific surface areas similar to that of P25 photoanodes, their efficiencies do not compare well against an average moderate 5−7% efficiency for DSSCs based on the P25 photoanodes.[33,34] The deficient performance may arise from the structures of these titania-coated FTO nanoparticle films. The FTO films are coated with TiO_2 using wet chemical or atomic layer deposition (ALD) techniques. There is no guarantee that all the FTO particle surfaces are coated with TiO_2.[23] As a result, the recombinations with electrolyte occur in the site without TiO_2 coatings. Furthermore, because of the small sizes of FTO nanoparticles, the continuity of the electron migration path via FTO nanoparticles may break before they extend to the substrate collector (Scheme 1a). In this case,

Scheme 1. Comparison of Photo-Injected Electron Tranportation Path in TiO_2-Treated FTO Samples[a]

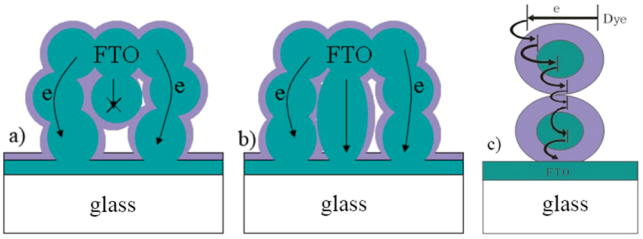

[a](a) Broken path and (b) continuous path. (c) Illustration of the pretreatment of titania on FTO particles; the outer TiO_2 layer disconnects the electron transport path between FTO particles.

electrons in FTO may hop between different TiO_2 coated FTO nanoparticles to find a new shortcut to the out circuit. Because the electrons reenter the TiO_2 shell, an electron transport path similar to random walking may reappear (Scheme 1a). So, it is important to receive a continuous electron transport chain with good titania coatings at the FTO surface for high-performance DSSCs based on titania-coated FTO as novel photoanode materials (Scheme 1b).

In the present work, micrometer- sized FTO particles are prepared and coated with TiO_2 for photoanode applications in DSSCs. Large FTO particles guarantee the continuous electron path to the collector. Intermittent TiO_2 coating processes favor the uniform and successive coatings on FTO surfaces. Current density (J_{sc} = 25.5 mA/cm^2), open circuit voltage (V_{oc} = 0.68 V), fill factor (FF = 44%), and efficiency (η = 7.8%) are received on cells with 8 μm thick TiO_2@FTO films, except for the low dye loadings, which are one-ninth of an ordinary level using P25 photoanodes. Electron impedance spectroscopy analyses reveal a high photoinjected charge transmission rate and low charge recombination at the interface.

RESULT AND DISCUSSION

FTO Particle Characterization. Typical powder X-ray diffraction (XRD) patterns for SnO_2 and fluorine-doped SnO_2 samples are illustrated in Figure 1a. All the diffraction peaks of the undoped and fluorine-doped samples can be well indexed to the rutile structure of SnO_2 (space group: *P*42/*mnm* (136), JCPDS No. 41-1445). SnO_2 does not change its structure after fluorine doping. F^- is reported to occupy O vacancy sites in SnO_2.[35] The presence of F^- in the SnO_2 lattice was confirmed from the energy-dispersive X-ray spectroscopy (EDX) analysis (Figure 1b). The atomic ratio of F/Sn is calculated to be about 1:5. FTO particles are in micrometer size, according to a representative scanning electron microscope (SEM) image (Figure S1a, Supporting Information). At higher magnification, we notice that these micrometer-sized FTO particles are composed of smaller particles (300−500 nm). The SEM image of photoanode film based on FTO particles is also shown in Figure S1b (Supporting Information). The resistivity of the as-prepared FTO samples is 0.2 Ω·m, detected by the Hall effect.

Two different kinds of photoanode were applied using the as-prepared FTO samples. The first one is to coat titania before film making, or pre-coating (Scheme 1c). The other one is to coat titania after film making, or post-coating (Scheme 1b). Comparing the efficiencies of pre-coating films and P25 films (Table 1), we find that the cell efficiency of 5.9% for the pre-coated samples is inferior to that of 7.0% for P25 films. The lower pre-coated film efficiency may be directly related to the fewer dye loadings in the pre-coated films. When dye is desorbed from the photoanodes and its concentration is characterized by UV−vis techniques, we find that the dye loadings in pre-coated films is one-seventh of that in P25 films. However, V_{oc} for both pre- and post-coated samples are much higher than that of mere SnO_2 photoanodes (around 450−480 mV) and very close to that of TiO_2-coated FTO photo-

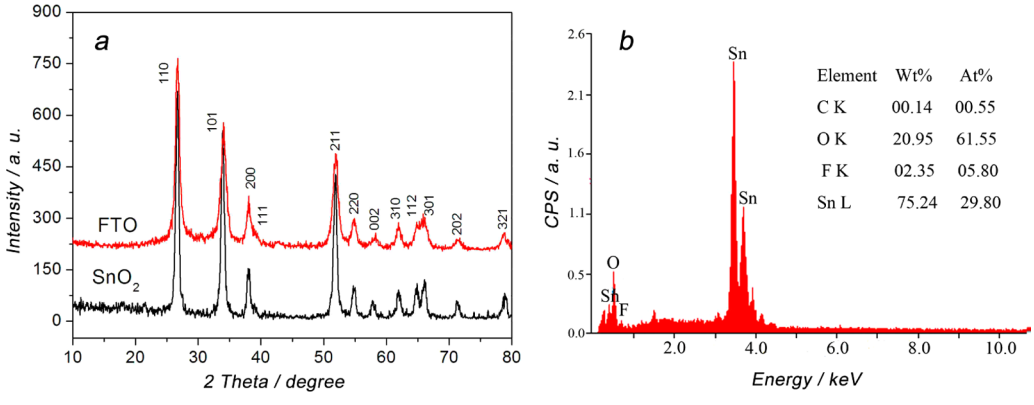

Figure 1. (a) XRD patterns of fluorine doped SnO_2 and SnO_2 particles. (b) EDX spectrum of the FTO particles.

Table 1. Photovoltaic Characteristics of Devices

electrodes	film thickness (μm)	coating cycles	J_{sc} (mA/cm^2)	V_{oc} (V)	FF (%)	η (%)	absorbed dye ($\times 10^{-7}$ mol/cm^3)	τ_e (ms)
pre-coated	8		21.3	0.57	49	5.9	0.39	283
P25	10		18.8	0.66	56	7.0	2.79	28
Bare FTO	3		11.4	0.36	38	1.4	0.10	41
post-coated	3	1	10.8	0.64	48	3.3	0.15	50
	3	2	13.8	0.67	52	4.8	0.19	283
	3	3	9.5	0.60	54	3.1	0.13	233
	3	4	7.9	0.63	48	2.3	0.10	504
	5	2	23.8	0.69	46	7.4	0.25	233
	8	2	24.9	0.64	42	6.7	0.32	131

anodes,[31,32] which suggests the good titania coverage on FTO microparticles.

It is now well-accepted that bifunctional photoelectrode materials can improve the efficiency of DSSCs, because the thin surface layer of nanocrystalline particles effectively absorb the dye and reduce the photoinjected charge recombination, enhancing the electron collection efficiency and thus improving the performance of the DSSCs. It is believed that the TiO_2 layer as an energy barrier is coated on the surface of FTO.[36] If the energy barrier is thin enough, it can be reputed as the electron injection layer, which has no effect on the electron injection from the excited dye into the photoelectrode film and yet prohibits the charge recombination with the oxidized dye or I_3^- in electrolyte. But if the layer is too thick, it greatly reduces the photo charge injection from excited dye through the TiO_2 layer into FTO films. So, we now discuss the results caused by the different TiO_2 deposition cycles.

Post-treatment films result in much better efficiency. First, we study the efficiency versus deposition cycles. The film thickness is kept at 3 μm for better surface coatings of FTO particles. When FTO particles are used directly as the photoanode, which corresponds to zero titania coating cycle, an ultralow dye loading is received. The FTO surface has a more acidic character and an isoelectric point at pH 4−5 (same as tin dioxide), which exceeds the TiO_2 surface isoelectric point of pH 6.2, and thus, bare FTO particle film adsorbs fewer dye molecules.[23,32] The low open circuit voltage of 0.36 V also represents the average V_{oc} of FTO photoanode, owing to the FTO and SnO_2 conduction bands that are more positive than that of TiO_2.[32,37]

When titania is coated onto FTO particles, apparent changes can be obtained. V_{oc} increases to 0.6−0.7 V, while J_{sc} also increases due to increased dye loadings. Post-titania-coated FTO films in 3 μm thickness with different coating cycles are subjected to the tests. When the cycle is 1, the deposited TiO_2 is too thin to absorb enough dye (0.15×10^{-7} mol/cm^3) and fully cover FTO particle films, which results in low J_{sc} (10.8 mA/cm^2) and low FF (48%). And when the cycle is 2, the photovolatic characteristics of the device are much better with short-circuit current density J_{sc}, open circuit voltage V_{oc}, and FF of 13.8 mA/cm^2, 0.67 V, and 52%, respectively. The more TiO_2 particles are deposited on FTO particles films, the more absorbance dyes (0.1×10^{-7} mol/cm^3) and the higher open voltage. However, as the cycles of titania treatment increases from 2 to 4, the open circuit voltage of DSSCs reduces. There exist several reasons for this phenomenon. The first is that the voids of mesoporous FTO films could be blocked by TiO_2 nanoparticles, resulting in a reduced specific surface area and thus lower dye loadings. At the same time, the electrolyte containing I^-/I_3^- redox couple was prevented from entering the pores. Furthermore, the mesoporous FTO films might be destroyed by increasing the number of cycles of immersion in $TiCl_4$ aqueous solution. So, in the present study, two deposition cycles of TiO_2 coating on the surface FTO particles is the optimal number of cycles for the cell performance.

Considering the thinner film and lower dye loadings, the result is much better than that for pre-coating samples. When the film thickness is further increased for the post-coated samples, efficiencies of 7.4 and 6.7% are obtained for 5 and 8 μm thick films. The lower fill factor for thicker film may be related to TiO_2 incompletely coated on FTO particles, which related the lower V_{oc} for 8 μm film.[23]

The efficiencies greater than 7% for over 5 μm thick post-titania FTO films is superior to that of P25 films, especially when much lower dye loading is taken into consideration. The great disparity of dye loading can be seen in the digital camera picture (Figure S3, Supporting Information). The highest dye loading of 0.32×10^{-7} mol/cm^3 for 8 μm thick post-titania-coating films is one-ninth that of 2.79×10^{-7} mol/cm^3 for P25 films. J_{sc} of 5 and 8 μm thick post-titania FTO films are 23.8 and 24.9 mA/cm^2, respectively, which are superior to that of P25. The power conversion efficiency of 7.4% based on 5 μm thick post-titania FTO films is higher than that of traditional P25 films and much higher than that for pretreated films. Considering the low dye loading levels, we attribute the enhanced cell performance to the better electron collections due to the direct electron migration path provided by the micrometer sized FTO particles, and we discuss this in the following section.

The superior properties for post-titania-treated cells benefit from its unique structures. The FTO particles are connected to generate a direct electron transport pathway to the out circuit prior to titania coating (Scheme 1b). A layer of titania is then coated onto the FTO particle films. The film may be described as titania-coated FTO film. In this configuration, direct electron migration to the outer circuit is favored only if electrons hop into FTO particles. Considering the micrometer size of FTO particles, this direct and continuous electron pathway may be easy to generate, because only limited layers of FTO particles are present in 5−8 μm thick films. On the contrary, if titania is coated onto FTO particles before film making, which prepares the titania-coated FTO core−shell structure, the entire outer layer of FTO particles is coated with titania. The photoanode films may be described as films of titania-coated FTO particles. Although the FTO core attracts electrons due to its excellent conductivity, it cannot provide a direct electron migration path to the outer circuit. Electrons are prone to hop between different titania-coated FTO particles.[37] In this case, random walkings similar to that in mere titania films cannot be totally excluded. This also explains the low efficiencies in the

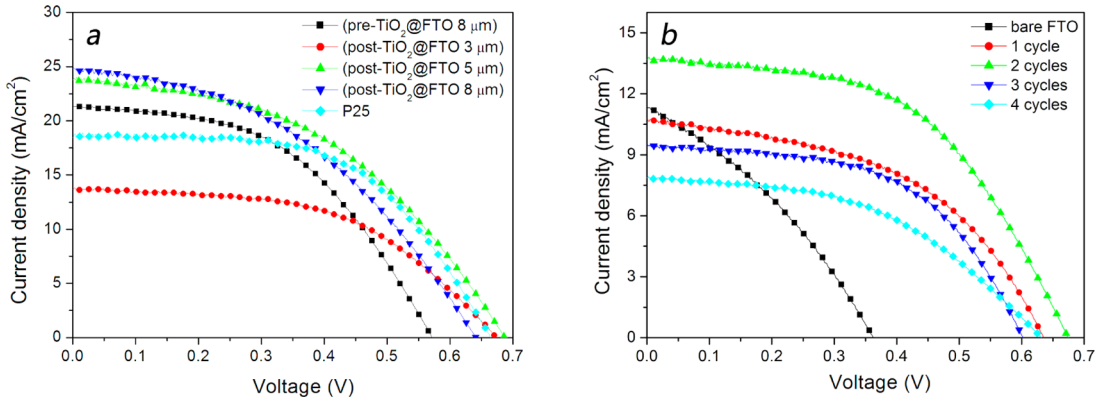

Figure 2. *J*–*V* curves for DSSCs based on (a) the different thicknesses of TiO_2@FTO film photoanodes and P25 photoanodes; (b) bare FTO films photoanodes and different TiO_2 deposition cycles coated on 3 μm FTO film photoanodes.

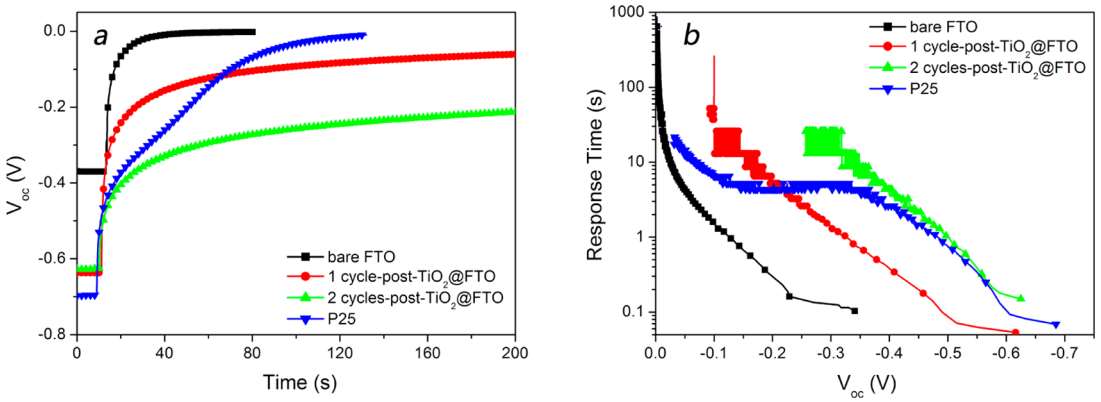

Figure 3. (a) Open-circuit voltage decay and (b) τ_n–V_{oc} curves of the DSSCs based on (black) bare FTO particles, (red) one cycle of post-deposition of TiO_2 on FTO, (green) two cycles of post-deposition of TiO_2 on FTO and (blue) P25 film.

literature.[37] As expected, the evaluation factors of DSSCs (summarized in Table 1 and Figure 2) give strong support that the better photoelectrode fabrication is post-treament of TiO_2 on FTO particles. Compared to 10 μm thick P25 photoanode DSSC, the conversion efficiency for 5 μm thick TiO_2 coated FTO photoanode DSSC increases from 7.0 to 7.4%.

Although the size of FTO particles in the present study is much larger than that in the literature,[31,32] the cell performance is much better. The reason may be related to the large particle size of present FTO particles. Compared to P25, FTO particles are much more difficult to sinter together to form uniform films. There should exist a lot of large pores in the film. A continuous electron transport path along FTO particles is likely to be broken. In this case, during the post-treatment, TiO_2 nanoparticles will fill these pores. In the discontinuous site, electrons will hop into TiO_2 to find a new path to the outer circuit (Scheme 1a). Extra energy is required when an electron hops from one nanoparticle to another. Meanwhile, the tiny particles in the photoanode films have other drawbacks. The pore diameter formed by nanoparticles is too small for TiO_2 coating. The pores may be plugged by TiO_2 deposition layer, decreasing effective surface, which is serious with increasing deposition cycles. On the contrary, when submicrometer-sized FTO particles are applied in the study, there are limited FTO particles along the film thickness direction, which favors the formation of a direct and continuous electron transport pathway. Larger FTO particles also leave large pores for TiO_2 treatment. Their surface is easier to be covered by TiO_2 post treatment. So, the cell efficiency of 5 μm thick TiO_2@FTO cell is superior to that of P25 cells.

The interfacial recombination of electron plays an important role for the DSSCs performance. The open-circuit voltage decay (OCVD) curve can qualitatively show the main information on the interfacial recombination processes between the photoinjected electrons in the photoelectrode materials and electrolyte.[38,39] The electron survival lifetime (τ_n) in DSSCs can change with the cell's open-circuit voltage (V_{oc}) due to the shift of semiconductor's quasi-Fermi level, which is dictated by the density of electrons in the conduction band.[40,41] Therefore, the electron recombination reaction can be qualitatively illustrated by analyzing the shapes of τ_n–V_{oc} relation curves. The relationship between electron survival lifetime (τ_n) and open circuit voltage decay is given by eq 1.[41,42]

$$\tau_n = \frac{\kappa_B T}{q}\left(\frac{dV_{OC}}{dt}\right)^{-1} \quad (1)$$

where κ_B is the Boltzmann constant, T is the temperature, and q is the electron charge.

In Figure 3, panel a depicts the open circuit voltage decay curves, and panel b depicts the τ_n–V_{oc} relation curves of the solar cells fabricated with bare FTO (black), one cycle postdeposition TiO_2 on interface FTO (red), two cycles postdeposition TiO_2 on interface FTO (green), and P25 film (blue) under open-circuit and dark conditions. As can be seen in Figure 3a, the V_{oc} values for the solar cells decay rapidly after ~5 s in the dark state, while the V_{oc} value for bare FTO-based

dx.doi.org/10.1021/am503074j | ACS Appl. Mater. Interfaces 2014, 6, 16593–16600

solar cell decays significantly to ~0 V after ~10 s. It is notable that V_{oc} values for P25 decays quickly from 0.3 to 0.15 V between ~20 and 50 s, compared to ~5 s after in the dark state, and then decay placidly from 0.15 to 0 V, which is a result of trapping and detrapping in internal titania at medium potential.[40] Meanwhile, V_{oc} values for one- and two-cycle TiO_2@ FTO remain at 0.1 and 0.3 V, respectively, after 200 s in the dark condition.

The τ_n–V_{OC} relation curves are shown in Figure 3b, which is derived from Figure 4a according to eq 1. As shown in Figure 3b, the electron survival lifetime (τ_n) shows an exponential dependence at the V_{oc}, and τ_n of the bare FTO-based solar cell is much lower than that of the P25-based solar cell, while τ_n of the two-cycle TiO_2@FTO-based solar cell is longer than the latter. It is obvious that τ_n of the one-cycle TiO_2@FTO-based solar cell is longer than that of P25-based solar cell in the low-voltage region. Therefore, the recombination stemming from the surface trapping and detrapping is much less in these two kinds of photoelectrode.[40] As discussed above, a photo-generated electron can be captured by FTO films and then directly transferred into a conductive substrate. So, there is much less recombination on the interface of deposited TiO_2/dye/electrolyte.These results are in good agreement with the below survey from the Bode plots in Figure 4b.

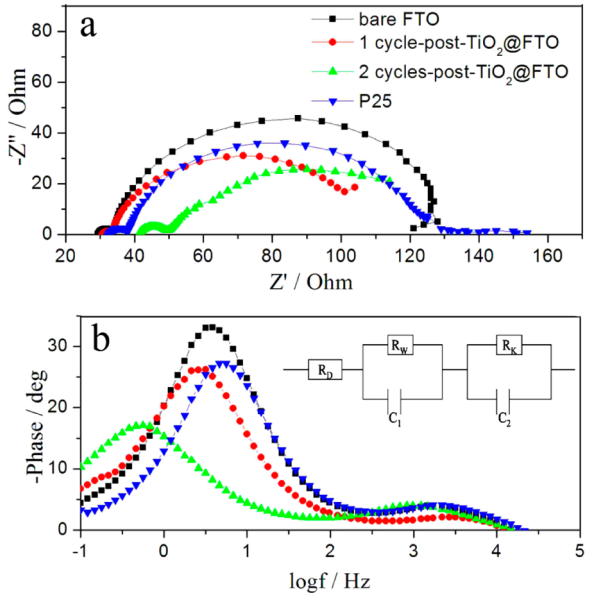

Figure 4. (a) Nyquist plot and (b) Bode plot and the equivalent circuit used for fitting data from electrochemical impedance spectroscopy (EIS) measured at open-circuit voltages of (black) bare FTO particles, (red) one cycle post-deposition TiO_2 on FTO interface, (green) two cycles post-deposition TiO_2 on FTO interface, (blue) and P25 film; R_D represents the serial resistance, which is mainly influenced by the sheet resistance of the substrate and electrical contact between the conductive FTO glass/TiO_2 interfaces; R_w represents the impedance with charge transfer at the platinum counter electrode or electrical contact between TiO_2 particles, and R_K represents the impedance related to charge transfer process at TiO_2/dye/electrolyte interfaces.

Electrochemical impedance spectroscopy (EIS) provides a deeper understanding on the interfacial charge transport in DSSCs.[43−45] To uncover the difference in the interfacial distinction of these photoelectrodes, we surveyed EIS spectra of the DSSCs at an applied bias of V_{oc} and a frequency range from 0.1 or 0.01 Hz to 1 MHz, with AC amplitude of 5 mV. Figure 4a,b displays EIS spectra of DSSCs based on different layers of TiO_2-coated FTO powder photoelectrodes. In all the Nyquist plots, two semicircles were well-defined in the high-frequency region (>1 kHz) and in the medium frequency region (100−1 Hz). It is generally accepted that an EIS spectrum has three semicircles; the first semicircle in the high-frequency region indicates the redox reaction of I^-/I_3^- at the Pt/electrolyte interface, the second semicircle expresses the electron transfer at the oxide/dye/electrolyte interface and the electron transport in the TiO_2@FTO photoelectrode, and the third shows the Warburg diffusion process of I^-/I_3^- in electrolyte. Usually, the second semicircle is the largest semicircle. In our case, the third is not well resolved and is hindered by the first and second semicircles. We then calculate the charge lifetime (τ_e) as the equality (2) of the two kinds of the DSSCs, where the f_{mid} is the maximum frequency in Bode plot. The proposed mechanism is reflected in the EIS data (the right column in Table 1).

$$\tau_e = 1/(2\pi f_{mid}) \quad (2)$$

The current of the device is subject to the charge collection efficiency. Efficient charge collection is a prerequisite for the efficient conversion of light to electrical energy. The effective electron diffusion length is indicated to describe charge collection efficiencies. The effective electron diffusion length can be calculated from[42]

$$L_e = \sqrt{D_n \tau_e} \quad (3)$$

Using values obtained from EIS, we found that bare FTO films and pre- or post-treatment FTO films had longer charge lifetimes (τ_e > 40 ms) than those of traditional P25 films (τ_e, 28 ms). So, the effective electron diffusion lengths of different FTO particles are superior to P25 films. The effective electron collection had been corresponding to the effective electron diffusion lengths. Bare FTO films and pre- or post- treatment FTO films have better charge collection efficiency, which results from the devices having better photovoltaic characteristics than the device based on P25 films. The traditional DSSCs based on P25 film as photoelectrode have an optimum film thickness of 8−14 μm.[46] So, we only studied 8 μm TiO_2@ FTO post-treatment films for the performance of DSSCs. We will research other devices based on thicker TiO_2@FTO post-treatment films in future.[15]

Figure 5 shows the photocurrent action spectrum of the solar cells based on bare FTO particles (black), one-cycle post-deposition TiO_2 on FTO interface (red), two-cycle post-deposition TiO_2 on FTO interface (green), and P25 film (blue). The incident photo-to-current conversion efficiency (IPCE) reached the maximum values at 520 nm. As can be seen, the IPCE values after coating the TiO_2 layers increase significantly from 32% to 48%. This can be ascribed to the addition of the TiO_2 layers coating FTO to reduce photo-electron recombination with excited dye and I_3^- in the electrolyte, while the IPCE values of the former (48%) remarkably exceeded that of P25-based solar cell (37%), which can be due to the excellent electrical conductivity of FTO films.

The photoinjection current (J_{inj}) is divided by the competition of photoelectron recombination and the efficiency of photoelectron injection, which is dependent on incident light intensity and dye absorbance. And short-circuit current (J_{sc}) is obtained by the competition of the photoinjection current (J_{inj})

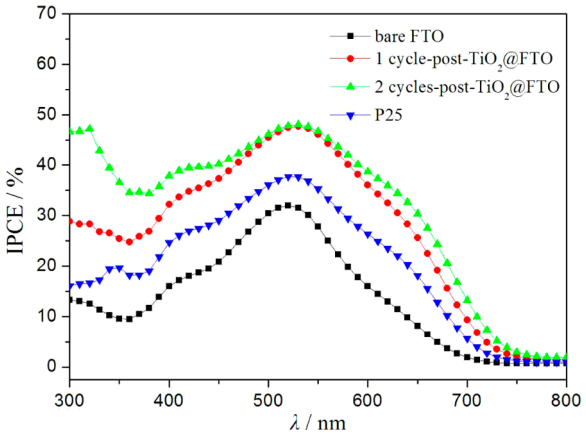

Figure 5. Photovoltaic action spectra for the DSSCs based on (black) bare FTO particles, (red) one-cycle post-deposition TiO_2 on FTO interface, (green) two-cycle post-deposition TiO_2 on FTO interface, (blue) and P25 film.

and the recombination current (J_{rec}), according to the following equation:[47,48]

$$J_{sc} = J_{inj} - J_{rec} \quad (4)$$

As we discussed above, DSSCs based on FTO films have a high effective photoinjection current (J_{inj}); furthermore, they also have a lower recombination current (J_{rec}) after being coated with TiO_2 layers. Therefore, solar cells based on two cycles TiO_2@FTO films photoanode have outstanding performance, compared to P25-based solar cells.

Long-term stability is one critical parameter that limits cell applications. We probed 5 and 8 μm post-treated TiO_2@FTO-film-based devices for 10 successive days under natural light at 50 °C, and the devices showed stable photovoltaic characteristics (Figure S3, Supporting Information). J_{sc} of 5 μm thick cell decreased from 23.8 to 19.4 mA/cm^2, and V_{oc} did not change much for 240 h, which may have been caused by electrolyte leakage. The latter J_{sc} for 10 μm thick cell increases to 25.5 mA/cm^2,[49] and the power conversion efficiency (η) increased from 6.7 to 7.6% as a consequence.

In summary, our research suggests a rapid collection of electrons in photoelectrodes for high cell performance. The continuous electron pathway by FTO particles is much more important than the specific surface area. TiO_2@FTO shell–core structure difunctional materials have been prepared and applied in dye-sensitized solar cells. FTO particles serve as a rapid electron transport channel for the photoinjected electron so as to increase the charge collection efficiency. TiO_2 deposition layers work as energy barrier and dye adsorption active site. Embodied by EIS, both bare FTO and TiO_2@FTO photoelectrodes exhibit a longer charge lifetime than that of P25 photoelectrode, which is a benefit of the high conductivity of FTO particles and the TiO_2 layer coated on the surface of the FTO particles. Compared to that of 10 μm thick P25 photoanode cells, 5 μm thick DSSCs with less than $^1/_{10}$ dye loadings based on TiO_2@FTO photoanodes show an overwhelming performance of 7.4%.

EXPERIMENTAL SECTION

Preparation of FTO Powders. The fluorine-doped tin oxide nanocrystalline powders were prepared by reported sol–gel techniques.[50] For the synthesis FTO nanopowder, 5 g of $SnCl_2 \cdot 2H_2O$ and 0.4 mL of 40% HF solution were dissolved in 100 mL of deionized water. The mixed solution was slowly added to a solution of 5 mL of acetylacetone in 14 mL of methanol with rapid stirring. The addition of the acetylacetone solution took about 45 min, while the rapid stirring was continued. The aqueous ammonia solution was added drop-wise to the mixed solution until a gel formed. The dropping rate must be well controlled (the optimum pH value of solution is 9.5) to obtain the chemical homogeneity. The resulting gel product was filtered and washed several times with cold water until Cl^- ions were entirely removed before the product was transferred to the oven for further drying at 100 °C. The absence of Cl^- ions was checked by 0.1 M $AgNO_3$ water solution. Dried material converted to alcogel by methanol, and powders of FTO were obtained in a furnace by calcination for 2 h at 600 °C.

Preparation of Mesopore TiO_2@FTO Films. Method 1 (Figure 2a): To prepare TiO_2-coated FTO core–shell structure particles, FTO (0.3 g, 0.002 mol) powders were immersed in 2 mM $TiCl_4$ aqueous solution for 1 h at 100 °C with constant stirring and then washed with distilled water to remove residual $TiCl_4$. We repeated the above process one time. TiO_2-coated FTO particles (0.3 g 0.002 mol) and ethyecellulose/terpinol (0.5 mL, 5 wt %) were pestled for 30 min in an agate mortar and then sonicated for 1 h. The TiO_2@ FTO paste was spread uniformly on the surface of the FTO glass using doctor-blade technique. The films of FTO particles were sintered at 450 °C in air for 30 min.

Method 2 (Figure 2b): To prepare a FTO paste, FTO (0.3 g) powder and ethyecellulose/terpinol (0.5 mL, 5 wt %) were pestled for 30 min in an agate mortar and then sonicated for 1 h. The FTO paste was spread uniformly on the surface of the FTO glass using doctor-blade technique. The films of FTO particles were sintered at 450 °C in air for 30 min. Coating of TiO_2 on the FTO films was performed by dipping the FTO electrodes into a 2 mM $TiCl_4$ aqueous solution for 1 h at 100 °C until the $TiCl_4$ was hydrolyzed. Then the films were washed with distilled water to remove residual $TiCl_4$ and dried at 100 °C in air for 4 h. The structures of mesopore TiO_2@FTO films are shown in Figure 2b.

Finally, the TiO_2@FTO electrodes prepared using Methods 1 and 2 were soaked in an ethanol solution containing 0.5 mM N719 dye for 2 days at room temperature, washed with ethanol, and dried in dry air. The DSSCs were fabricated from the dye-absorbed oxide photoanode placed on a Pt sputtered conducting glass consisting of a 100 μm thick thermal adhesive film as a separating layer. The electrolyte composition was a mixture of 0.3 M DMHImI, 0.5 M LiI, 0.05 M I_2, and 0.5 M *tert*-butylpyridine (TBP) in acetonitrile. The active areas of the photoanodes were about 0.16 cm^2 with aluminum film. Not otherwise specified, the thickness of FTO particles films is 3 μm. Furthermore, the IPCE and OCVD are measured from the devices based on 8 μm FTO particles films.

Characterizations. The phase of the FTO powders were characterized by XRD using a Rigaku (Japan) D/Max2550VB+/PC X-ray diffractometer equipped with Cu Kα radiation (λ = 1.5418 Å) at a scanning rate of 5°/min for 2θ ranging from 10 to 80°. The operation voltage and current were 40 kV and 40 mA, respectively. The size, morphology, and thickness of the FTO particle films were observed using a Philips-FEI Quanta 200 SEM with an operation voltage of 20 kV.

Measurement of Photovoltaic Characterizations. A 350W xenon light source (ShangHai) was used to provide the J–V and P–V curves under an incident irradiance of AM 1.5 (100 mW/cm^2) for solar cells. EIS analyses were conducted with the bias voltage set at the open-circuit voltage (V_{oc}) and the frequency set from 0.01 Hz to 100 kHz with oscillation amplitude of 5 mV at AM 1.5 (100 mW/cm^2). The OCVD measurement used electrochemical workstations (CHI660D, ShangHai) at AM 1.5 (100 mW/cm^2), and then we turned off the light to perform the test under dark conditions. The OCVD curve was recorded and further transformed in the corresponding electron survival lifetime (τ_n)–open circuit voltage (V_{OC}) relation curve. The IPCE was measured as a function of wavelength from 300 to 800 nm by using CROWNTECH Q-test station 500TI. The N719 dye absorbed on the TiO_2 films was obtained by using the UV–vis–NIR spectrophotometer (TU-1901, Beijing).

The model Hall effect measurement system was an HMS-300 made by ECOPIA company (Korea). The current and magnetic field strength were 10 μA and 0.560 T, respectively, at 300 K. FTO samples were pressed into pellets for the tests.

■ ASSOCIATED CONTENT

Supporting Information

SEM images of FTO particle and films, top-view and cross-sectional view of the photoanodes with different thicknesses, digital camera pictures for dye loading comparison, $J-V$ curves tested after 10 days, and Bode plots for DSSCs based on different cycles TiO_2 deposited on FTO surface. This material is available free of charge via the Internet at http://pubs.acs.org.

■ AUTHOR INFORMATION

Corresponding Author

*E-mail: jhzeng@ustc.edu.

Notes

The authors declare no competing financial interest.

■ ACKNOWLEDGMENTS

This work was supported by the Natural Science Foundation of China (No. 21071093), the Fundamental Research Funds for the Central Universities (Grant No. GK201402017) from the Department of Education (DoE), and the outstanding doctoral dissertation project of Shaanxi Normal University (Grant No. S2012YB03).

■ REFERENCES

(1) Law, M.; Greene, L. E.; Johnson, J. C.; Saykally, R.; Yang, P. D. Nanowire Dye-Sensitized Solar Cells. *Nat. Mater.* **2005**, *5*, 455−459.

(2) Snaith, H. J.; Humphry-Baker, R.; Chen, P.; Cesar, I.; Zakeeruddin, S. M.; Grätzel, M. Charge Collection and Pore Filling in Solid-State Dye-Sensitized Solar Cells. *Nanotechnol.* **2008**, *19*, 424003.

(3) Brown, P.; Takechi, K.; Kamat, P. V. Single-Walled Carbon Nanotube Scaffolds for Dye-Sensitized Solar Cells. *J. Phys. Chem. C* **2008**, *112*, 4776−4782.

(4) Grätzel, M. Photoelectrochemical Cells. *Nature* **2001**, *414*, 338−344.

(5) Nelson, J. Continuous-Time Random-Walk Model of Electron Transport in Nanocrystalline TiO_2 Electrodes. *Phys. Rev. B* **1999**, *59*, 15374−15380.

(6) Kopidakis, S.; Schiff, E. A.; Park, N. G.; van de Lagemaat, J.; Frank, A. J. Ambipolar Diffusion of Photocarriers in Electrolyte-Filled Nanoporous TiO_2. *J. Phys. Chem. B* **2000**, *104*, 3930−3936.

(7) Peter, L. "Sticky Electrons" Transport and Interfacial Transfer of Electrons in the Dye-Sensitized Solar Cell. *Acc. Chem. Res.* **2009**, *42*, 1839−1847.

(8) Maggio, E.; Martsinovich, N.; Troisi, A. Theoretical Study of Charge Recombination at the TiO_2-Electrolyte Interface in Dye Sensitized Solar Cells. *J. Chem. Phys.* **2012**, *137*, 22A508.

(9) Nakade, S.; Matsuda, M.; Kambe, S.; Saito, Y.; Kitamura, T.; Sakata, T.; Wada, Y.; Mori, H.; Yanagida, S. Dependence of TiO_2 Nanoparticle Preparation Methods and Annealing Temperature on the Efficiency of Dye-Sensitized Solar Cells. *J. Phys. Chem. B* **2002**, *106*, 10004−10010.

(10) Hao, F.; Wang, X.; Zhou, C.; Jiao, X. J.; Li, X.; Li, J. B.; Lin, H. Efficient Light Harvesting and Charge Collection of Dye-Sensitized Solar Cells with (001) Faceted Single Crystalline Anatase Nanoparticles. *J. Phys. Chem. C* **2012**, *116*, 19164−19172.

(11) Ke, C. R.; Chen, L. C.; Ting, J. M. Photoanodes Consisting of Mesoporous Anatase TiO_2 Beads with Various Sizes for High-Efficiency Flexible Dye-Sensitized Solar Cells. *J. Phys. Chem. C* **2012**, *116*, 2600−2607.

(12) Yanagida, M.; Numata, Y.; Yoshimatsu, K.; Ochiai, M.; Naito, H.; Han, L. Y. Structure of Electron Collection Electrode in Dye-Sensitized Nanocrystalline TiO_2. *Electrochim. Acta* **2013**, *87*, 309−316.

(13) Tan, B.; Wu, Y. Y. Dye-Sensitized Solar Cells Based on Anatase TiO_2 Nanoparticle/Nanowire Composites. *J. Phys. Chem. B* **2006**, *110*, 15932−15938.

(14) Liu, B.; Aydil, E. S. Growth of Oriented Single-Crystalline Rutile TiO_2 Nanorods on Transparent Conducting Substrates for Dye-Sensitized Solar Cells. *J. Am. Chem. Soc.* **2009**, *131*, 3985−3990.

(15) Xu, C. K.; Wu, J. M.; Desai, U. V.; Gao, D. Multilayer Assembly of Nanowire Arrays for Dye-Sensitized Solar Cells. *J. Am. Chem. Soc.* **2011**, *133*, 8122−8125.

(16) Wang, S. M.; Dong, W. W.; Tao, R. H.; Deng, Z. H.; Shao, J. Z.; Hu, L. H.; Zhu, J.; Fang, X. D. Optimization of Single-Crystal Rutile TiO_2 Nanorod Arrays Based Dye-Sensitized Solar Cells and Their Electron Transport Properties. *J. Power Sources* **2013**, *235*, 193−201.

(17) Zhang, C. N.; Chen, S. H.; Mo, L. E.; Huang, Y.; Tian, H. J.; Hu, L. H.; Huo, Z. P.; Dai, S. Y.; Kong, F. T.; Pan, X. Charge Recombination and Band-Edge Shift in the Dye-Sensitized Mg^{2+}-Doped TiO_2 Solar Cells. *J. Phys. Chem. C* **2011**, *115*, 16418−16424.

(18) Prasittichai, C.; Hupp, J. T. Surface Modification of SnO_2 Photoelectrodes in Dye-Sensitized Solar Cells: Significant Improvements in Photovoltage via Al_2O_3 Atomic Layer Deposition. *J. Phys. Chem. Lett.* **2010**, *1*, 1611−1615.

(19) Chandiran, A. K.; Sauvage, F.; Casas-Cabanas, M.; Comte, P.; Zakeeruddin, S. M.; Grätzel, M. Doping a TiO_2 Photoanode with Nb^{5+} to Enhance Transparency and Charge Collection Efficiency in Dye-Sensitized Solar Cells. *J. Phys. Chem. C* **2010**, *114*, 15849−15856.

(20) Lu, X. J.; Mou, X. L.; Wu, J. J.; Zhang, D. W.; Zhang, L. L.; Huang, F. Q.; Xu, F. F.; Huang, S. M. Improved-Performance Dye-Sensitized Solar Cells Using Nb-Doped TiO_2 Electrodes: Efficient Electron Injection and Transfer. *Adv. Funct. Mater.* **2010**, *20*, 509−515.

(21) Duan, Y. D.; Fu, N. Q.; Liu, Q. P.; Fang, Y. Y.; Zhou, Xi. W.; Zhang, Ji. B.; Lin, Y. Sn-Doped TiO_2 Photoanode for Dye-Sensitized Solar Cells. *J. Phys. Chem. C* **2012**, *116*, 8888−8893.

(22) Feng, X. J.; Shankar, K.; Paulose, M.; Grimes, C. A. Tantalum-Doped Titanium Dioxide Nanowire Arrays for Dye Sensitized Solar Cells with High Open-Circuit Voltage. *Angew. Chem., Int. Ed.* **2009**, *48*, 8095−8098.

(23) Kay, A.; Grätzel, M. Dye-Sensitized Core-Shell Nanocrystals: Improved Efficiency of Mesoporous Tin Oxide Electrodes Coated with a Thin Layer of an Insulating Oxide. *Chem. Mater.* **2002**, *14*, 2930−2935.

(24) Wang, Z. C.; Luo, J. B.; Cao, A. Y.; Wu, D. H. Double-Walled Carbon Nanotube Solar Cells. *Nano Lett.* **2007**, *7*, 2317−2321.

(25) Hu, L. B.; Kim, H. S.; Lee, J. Y.; Peumans, P.; Cui, Y. Scalable Coating and Properties of Transparent, Flexible, Silver Nanowire Electrodes. *ACS Nano* **2010**, *4*, 2955−2963.

(26) Chen, T. Y.; Fan, C. M.; Wu, J. Y.; Lin, T. L. Hybrid Silver Nanowire/Titanium Oxides Nanocomposites as Anode for Dye-Sensitized Solar Cell Application. *J. Chin. Chem. Soc.* **2009**, *56*, 1244−1249.

(27) Wang, Y. F.; Zeng, J. H.; Li, Y. Silver/Titania Nanocable as Fast Electron Transport Channel for Dye-Sensitized Solar Cells. *Electrochim. Acta* **2013**, *87*, 256−260.

(28) Wang, Y. F.; Sheng, X. Y.; Jin, B. B.; Zeng, J. H. A Performance Enhancement by Ag/C Nanocables in Photo-Anodes for Dye-Sensitized Solar Cells. *Energy Environ. Focus* 2014, accepted. DOI: 10.1166/eef.2014.1123.

(29) Wang, H. W.; Ting, C. F.; Hung, M. K.; Chiou, C. H.; Liu, Y. L.; Liu, Z. W.; Ratinac, K. R.; Ringer, S. P. Three-Dimensional Electrodes for Dye-Sensitized Solar Cells: Synthesis of Indium-Tin-Oxide Nanowire Arrays and ITO/TiO_2 Core−Shell Nanowire Arrays by Electrophoretic Deposition. *Nanotechnology* **2009**, *20*, 055601.

(30) Liao, H. C.; Lin, C. C.; Chen, Y. W.; Liu, T. C.; Chen, S. Y. Improvement in Photovoltaic Performance for Hybrid P3HT/Elongated CdS Nanocrystals Solar Cells with F-Doped SnO_2 Arrays. *J. Mater. Chem.* **2010**, *20*, 5429−5435.

(31) Yang, Z. Z.; Gao, S. M.; Li, T.; Liu, F. Q.; Ren, Y.; Xu, T. Enhanced Electron Extraction from Template-Free 3D Nanoparticulate Transparent Conducting Oxide (TCO) Electrodes for Dye-Sensitized Solar Cells. *ACS Appl. Mater. Interfaces* **2012**, *4*, 4419−4427.
(32) Icli, K. C.; Yavuz, H. I.; Ozenbas, M. Production of Core-Shell Type Conducting FTO/TiO_2 Photoanode for Dye Sensitized Solar Sells. *J. Solid State Chem.* **2014**, *210*, 22−29.
(33) Wang, Q.; Ito, S.; Grätzel, M.; Fabregat-Santiago, F.; Mora-Seró, I.; Bisquert, J.; Bessho, T.; Imai, H. Characteristics of High Efficiency Dye-Sensitized Solar Cells. *J. Phys. Chem. B* **2006**, *110*, 25210−25221.
(34) Qian, J. F.; Liu, P.; Xiao, Y.; Jiang, Y.; Cao, Y. L.; Ai, X. P.; Yang, H. X. TiO_2-Coated Multilayered SnO_2 Hollow Microspheres for Dye-Sensitized Solar Cells. *Adv. Mater.* **2009**, *21*, 3663−3667.
(35) Avadhut, Y. S.; Weber, J.; Hammarberg, E.; Feldmann, C.; Schellenberg, I.; Pöttgen, R.; Günne, J. S. Study on the Defect Structure of SnO_2:F Nanoparticles by High-Resolution Solid-State NMR. *Chem. Mater.* **2011**, *23*, 1526−1538.
(36) Palomares, E.; Clifford, J. N.; Haque, S. A.; Lutz, T.; Durrant, J. R. Control of Charge Recombination Dynamics in Dye Sensitized Solar Cells by the Use of Conformally Deposited Metal Oxide Blocking Layers. *J. Am. Chem. Soc.* **2003**, *125*, 475−482.
(37) Chappel, S.; Chen, S.; Zaban, A. TiO_2-Coated Nanoporous SnO_2 Electrodes for Dye-Sensitized Solar Cells. *Langmuir* **2002**, *18*, 3336−3342.
(38) Fan, K.; Peng, T. Y.; Chen, J. N.; Zhang, X. H.; Li, R. J. A Simple Preparation Method for Quasi-Solid-State Flexible Dye-Sensitized Solar Cells by Using Sea Urchin-Like Anatase TiO_2 Microspheres. *J. Power Sources* **2013**, *222*, 38−44.
(39) Xu, J. L.; Li, K.; Shi, W. Y.; Li, R. J.; Peng, T. Y. Rice-Like Brookite Titania as an Efficient Scattering Layer for Nanosized Anatase Titania Film-Based Dye-Sensitized Solar Cells. *J. Power. Sources* **2014**, *260*, 233−242.
(40) Bisquert, J.; Zaban, A.; Greenshtein, M.; Mora-Seró, I. Determination of Rate Constants for Charge Transfer and the Distribution of Semiconductor and Electrolyte Electronic Energy Levels in Dye-Sensitized Solar Cells by Open-Circuit Photovoltage Decay Method. *J. Am. Chem. Soc.* **2004**, *126*, 13550−13559.
(41) Zaban, A.; Greenshtein, M.; Bisquert, J. Determination of the Electron Lifetime in Nanocrystalline Dye Solar Cells by Open-Circuit Voltage Decay Measurements. *ChemPhysChem* **2003**, *4*, 859−864.
(42) Williams, V. O.; Jeong, N. C.; Prasittchai, C.; Farha, O. K.; Pellin, M. J.; Hupp, J. T. Fast Transporting ZnO-TiO_2 Coaxial Photoanodes for Dye-Sensitized Solar Cells Based on ALD-Modified SiO_2 Aerogel Frameworks. *ACS Nano* **2012**, *7*, 6185−6196.
(43) Yang, Z. Z.; Xu, T.; Gao, S. M.; Welp, U.; Kwok, W. K. Enhanced Electron Collection in TiO_2 Nanoparticle-Based Dye-Sensitized Solar Cells by an Array of Metal Micropillars on a Planar Fluorinated Tin Oxide Anode. *J. Phys. Chem. C* **2010**, *114*, 19151−19156.
(44) Fabregat-Santiago, F.; Bisquert, J.; Garcia-Belmonte, G.; Boschloo, G.; Hagfeldt, A. Influence of Electrolyte in Transport and Recombination in Dye-Sensitized Solar Cells Studied by Impedance Spectroscopy. *Sol. Energy Mater. Sol. Cells* **2005**, *87*, 117−131.
(45) Irvine, J. T. S.; Sinclair, D. C.; West, A. R. Electroceramics: Characterization by Impedance Spectroscopy. *Adv. Mater.* **1990**, *2*, 132−138.
(46) Mathew, A.; Rao, G. M.; Munichandraiah, N. Effect of TiO_2 Electrode Thickness on Photovoltaic Properties of Dye-Sensitized Solar Cell Based on Randomly Oriented Titania Nanotubes. *Mater. Chem. Phys.* **2011**, *127*, 95−101.
(47) Duong, T. T.; Choi, H. J.; He, Q. J.; Le, A. T.; Yoon, S. G. Enhancing the Efficiency of Dye-Sensitized Solar Cells With an SnO_2 Blocking Layer Grown by Nanocluster Deposition. *J. Alloys Compd.* **2013**, *561*, 206−210.
(48) Green, A. N. M.; Palomares, E.; Haque, S. A.; Kroon, J. M.; Durrant, J. R. Charge Transport versus Recombination in Dye-Sensitized Solar Cells Employing Nanocrystalline TiO_2 and SnO_2 Films. *J. Phys. Chem. B* **2005**, *109*, 12525−12533.
(49) Wang, Z. S.; Cui, Y.; Hara, K.; Dan-oh, Y.; Kasada, C.; Shinpo, A. A High-Light-Harvesting-Efficiency Coumarin Dye for Stable Dye-Sensitized Solar Cells. *Adv. Mater.* **2007**, *19*, 1138−1141.
(50) Senthilkumar, V.; Vickraman, P.; Ravikumar, R. Synthesis of Fluorine-Doped Tin Oxide Nanoparticles by Sol−Gel Technique and Their Characterization. *J. Sol−Gel Sci. Technol.* **2010**, *53*, 316−321.